Alfvén ion–ion hybrid wave heating in the Phaedrus-T tokamak

T. Intrator, P. H. Probert, M. Vukovic, S. Wukitch, A. Elfimov, R. Durst, R. A. Breun, D. Brouchous, D. Diebold, M. Doczy, R. Fonck, N. Hershkowitz, M. Kishinevsky, C. Litwin, R. Majeski, P. Nonn, and G. Winz
Department of Nuclear Engineering and Engineering Physics, University of Wisconsin, Madison, Wisconsin 53706-1687

(Received 14 July 1995; accepted 9 January 1996)

In the Phaedrus-T tokamak [R. A. Breun *et al.*, Fusion Technol. **19**, 1327 (1991)], Alfvén waves are indirectly driven by a fast wave antenna array. Small fractions of minority ions are shown to have a large effect on the Alfvén spectrum, as measured at the edge. An ion–ion hybrid Alfvén mode has been identified by measuring dispersion properties. Landau damping is predicted to be large and spatially localized. These Alfvénic waves are experimentally shown to generate correlated electron heating and changes in density near the core of the tokamak plasma. Fast wave antenna fields can mode convert at a hybrid Alfvén resonance and provide a promising route to spatially localized tokamak heating and current drive, even for low effective ionic charge $Z_{\mathrm{eff}}\approx 1.3$–2.
 [S1070-664X(96)00804-3]

I. INTRODUCTION

For a magnetized plasma with gradients in density or magnetic field, there have been many theoretical predictions that Alfvén waves can have a resonance[1] and heat the electrons at a spatially localized surface.[2,3] Some examples include the solar corona,[4] in a tokamak,[5] and in auroral arcs.[6] In a tokamak, electron heating and current drive in the Alfvén regime is accessible using ICRF (ion cyclotron range of frequencies) fast wave antenna heating systems that take advantage of mode conversion from antenna launched fast magnetosonic wave fields.

In the Phaedrus-T tokamak Alfvén waves are indirectly driven by a fast wave antenna array, and can generate electron heating in the plasma core. A low-power frequency sweep experiment was used to measure the dispersion properties. This wave behaves like an Alfvénic wave associated not with the nominally pure hydrogen ion species, but with an ion–ion hybrid Alfvén continuum. The presence of impurity ions such as fully stripped C^{VI}, D^{+} create a gap in the dispersion curve near the ion minority gyrofrequency and add another mode above the ion–ion hybrid frequency.

A radio-frequency (RF) power pulse experiment along with Beam Emission Spectroscopy (BES) identified a local (5–6 cm radial width) RF power deposition region at the core, as predicted. The exploration of advanced tokamak operating regimes will require off axis current drive (CD) to maintain reversed shear in the safety factor (q), which also appears to lead to desirable reduced radial transport properties. For this reason the radial localization of the RF power deposition attainable with the scenario we demonstrate here may turn out to be useful for other tokamak off axis CD experiments.

Here we show experimental data from related experiments at both high and low ICRF power. Core electron heating from ICRF waves is demonstrated at high power. At low power we show that small impurity fractions, e.g., effective ionic charge $Z_{\mathrm{eff}}\approx 1.3$–2 induce large changes from the single species Alfvén spectrum. This may help to explain a number of laboratory measurements, including Alfvén resonant heating,[7,8] antenna loading,[9] and wave fields in tokamaks[10] that have been carried out with nominally "pure" hydrogen plasmas. Impurity or minority ion effects may be very difficult to avoid when explaining the interactions of the Alfvén wave with plasma electrons. A cylindrical model appears to be adequate to explain the data shown in this paper, even though the Phaedrus-T tokamak has significant toroidicity at an aspect ratio $A\approx 3.7$, leading one to expect toroidal effects.

The connections between ion–ion hybrid waves and the fact that they are due to hybrid effects on the Alfvén spectrum have not received much attention. The recent success with mode conversion heating in the Tokamak Fusion Test Reactor[11] (TFTR) has generated more interest in this type of regime. Scenarios where fast wave antenna fields mode convert to an ion–ion hybrid Alfvén resonance promise routes to tokamak heating and current drive.

II. ALFVÉN AND ALFVÉN-ION–ION-HYBRID MODES

In the usual picture of the Alfvén resonance, the cylindrically symmetric density and B_θ gradients allow the local Alfvén speed $v_{\mathrm{A}}(r)=B(r)/[\mu_0 m_i n(r)]^{1/2}$ and frequency $\omega_{\mathrm{A}}(r)$ to match the pump field phase speed $v_{\phi z}$,

$$\omega_{\mathrm{A}}^2(r)=\frac{[n+m/q(r)]^2}{R^2}\left(1-\frac{\omega_{\mathrm{A}}^2(r)}{\omega_{ci}^2}\right)v_{\mathrm{A}}^2(r), \tag{1}$$

where the parallel helical wave number $k_\parallel=(n+m/q)/R$ is derived from toroidal and azimuthal mode numbers n and m, the ion cyclotron frequency is $\omega_{ci}(r=0)$, and the safety factor is $q(r)=rB_0/R_0B_\theta$. Here the toroidal magnetic field $B_0=B_{\mathrm{tor}}(R=R_0)$ and the major radius R_0 are considered to be fixed. A schematic of this geometry is shown in Fig. 1, where the antennas in the experiment are located on the low-field side, although the cylinder model cannot distinguish between the high- and low-field side. If $v_{\phi z}<v_e$, theory predicts[12–15] mode conversion to a kinetic Alfvén wave (KAW), with substantial Landau damping onto the electrons.

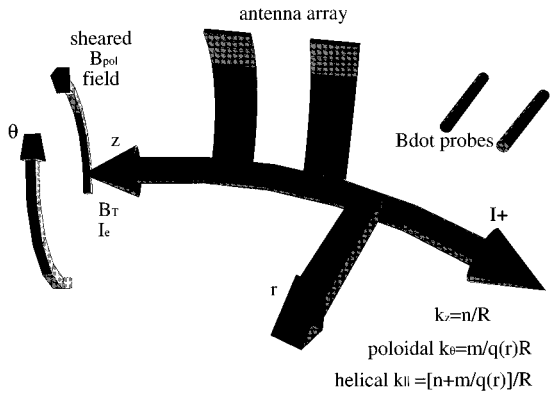

FIG. 1. Schematic of the basic cylindrical geometry including the toroidal, poloidal, radial, and (helical) parallel directions, along with the associated wave numbers. The antenna array straps are situated on the low-field side, and the sheared B_θ field is also indicated.

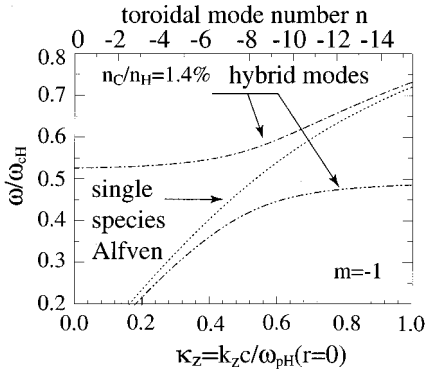

FIG. 2. Calculated slab model dispersion relation for the single species Alfvén waves (dotted line) given in Eq. (6), and the two hybrid branches, including the Alfvénic (dash–dot–dotted) ion–ion hybrid (dash–dotted) modes.

In the above high RF power heating experiment, the ion species mix consisted of a majority H, with a heavier minority of impurity carbon that could not be reduced below $n_C/n_H \approx 1\%-2\%$. Our suspicion that the observed electron heating was due to an Alfvénic ion–ion hybrid wave motivated a series of low RF power wave physics experiments. We added heavier ion species fractions such as deuterium, and covered the range $n_D/n_H \approx 0\%-200\%$. The results of these low-power experiments are shown in Sec. V, and make a case that the mode converted wave is an Alfvén wave associated, not with the nominally pure hydrogen ion species, but with a minority species ion–ion hybrid Alfvén continuum. These ion–ion hybrid waves occur at frequencies above the ion–ion hybrid[16] frequency ω_{ii},

$$\frac{\omega_{ii}^2}{\omega_{c2}^2}=\frac{1+\rho_z/\Omega_z}{1+\rho_z\Omega_z}, \tag{2}$$

where the ion gyrofrequencies for species 1 and 2 are ω_{c1} and ω_{c2}, $\rho_z=n_z m_z/(n_H m_H)$ and $\Omega_z=\omega_{c2}/\omega_{c1}=Zm_H/m_z$ are, respectively, the mass density and gyrofrequency ratios for ion species 2 with respect to ion species 1 (species 1 is hydrogen here).

The theoretically expected dispersion for the pure H Alfvén continuum from Eq. (1),

$$\frac{\omega}{\omega_{cH}}=\frac{\pm\kappa_{||}}{(1+\kappa_{||}^2)^{1/2}}, \tag{3}$$

asymptotes to $\omega \approx \omega_{cH}$ as $\kappa_{||}$ gets large. The toroidal and parallel wave numbers k_z and $k_{||}$ are normalized to the ion skin depth at $r=0$ so that $\kappa_z = k_z c/\omega_{pH}(r=0)$ and $\kappa_{||} = k_{||}c/\omega_{pH}(r=0)$, where ω_p is the ion plasma frequency. Since the Alfvén wave has flux surface symmetry and follows helical magnetic field lines, our launched k_z has a corresponding theoretical parallel wave number,

$$k_{||}=k_z+\frac{m}{q(r)R_0}=\frac{n+m/q(r)}{R_0}, \tag{4}$$

where n and m are, respectively, the toroidal and poloidal mode numbers. This dispersion relation is shown by the dotted line in Fig. 2.

The presence of impurity ions such as C, D adds another mode to the Alfvén continuum dispersion[17] above $\omega > \omega_{ii}$, and a gap at the ion gyrofrequency of the minority species $\omega_{c2} < \omega < \omega_{ii}$, along with the Alfvén branch associated with the lower gyrofrequency ion, and changes the discrete Alfvén spectrum as well.[12] The two branches are shown schematically in Fig. 2, where for simplicity we will refer to the lower branch as Alfvénic (dash–dot–dotted) and the upper one as the hybrid branch (dash–dotted).

The perpendicular resonance including the sum over minority ion species contributions corresponds to $N_{||}^2=S$, where

$$S=1+\sum_\sigma \frac{\omega_{p\sigma}^2}{\omega_{c\sigma}^2-\omega^2}, \tag{5}$$

and the subscript σ refers to all the electron and ion species, and we use the usual Stix notation.[18] This approach was used by Elfimov[12] *et al.* for a cold plasma cylinder approximation for the hybrid Alfvén continuum. The Alfvén hybrid frequency spectrum normalized to the hydrogen cyclotron frequency as a function of wave number is then[12]

$$\left(\frac{\omega_{AH}^{\pm}}{\omega_{cH}}\right)^2 = \frac{1+\rho_z+\xi\pm\{(1+\rho_z+\xi)^2-4\kappa_{||}^2[\rho_z+A^2(1+\kappa_{||}^2)]\}^{1/2}}{2[\rho_z+A^2(1+\kappa_{||}^2)]}, \tag{6}$$

where $A=\Omega_z^{-1}=m_z/Zm_H$, $\xi=\kappa_{||}^2(1+A^2)$.

For our electron heating experiment, the antenna was on the low-field side, the majority species 1 was H, the hydrogen gyrofrequency $\omega = \omega_{c1} = \omega_{cH}$ was outside the low-field side limiter, and the minority cyclotron $\omega=\omega_{c2}$ and hybrid $\omega=\omega_{ii}$ frequencies were just inside the high-field side limiter. In Fig. 3 we show slab model radial profiles of some typical experimental parameters for 1.4% carbon C^{VI} impurity minority in a hydrogen plasma, $B_0=0.67$ T, $\langle n_e\rangle = 8\times10^{18}$ m^{-3}, RF frequency of 7 MHz, launched

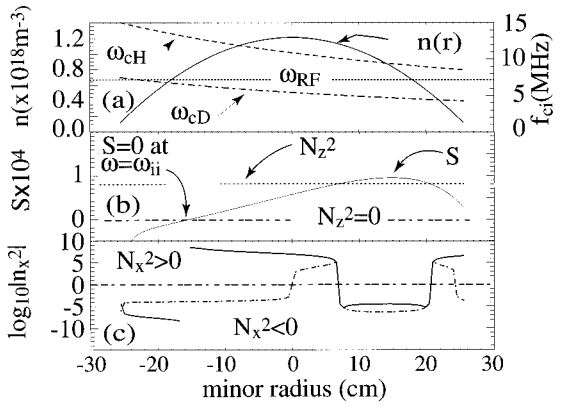

FIG. 3. Slab model plasma and calculated parameters as a function of minor radius with $r>0$ on the low-field side, including (a) density $n(r)$ (solid line), majority gyrofrequency (dashes), minority gyrofrequency (dash–dotted), launched RF frequency; (b) calculated Stix parameter S (solid), launched refractive index $n_z \approx 90$, $n_z^2 \approx 8100$, the location of the ion–ion hybrid frequency at $S=0$; and (c) calculated perpendicular refractive index n_x^2 with both slow (solid) and fast wave roots (dash–dotted), where $n_x^2<0$ corresponds to evanescent fields and $n_x^2>0$ corresponds to propagating waves.

$k_z \approx 0.12$ cm^{-1}. The density profile (solid line) and majority (dashes) and minority (dash–dotted) gyrofrequencies as a function of minor radius are indicated in Fig. 3(a). The limiters and antennas are located at $r=+25.5$ cm. In Fig. 3(b) we show the calculated local values of the Stix parameter S (solid line), the launched value of N_z^2 (dots), and indicate the nominal Alfvénic resonance at $N_z^2=S$, along with the location of the conventional Buchsbaum–Bers[16] ion–ion hybrid resonance at $S=0$ with $\omega=\omega_{ii}$. The conventional picture of minority ion–ion hybrid heating would lead to high-field side edge ion heating and not our experimentally observed core electron heating. In Fig. 3(c) we show for a given $N_z=90$ the calculated cold plasma slab model parallel refractive indices N_x^2 for both the slow (solid line) and fast (dash–dotted) wave roots. The fast wave is evanescent at the low-field side edge near the antenna ($N_x^2<0$), and we see the slab model Alfvén ion–ion hybrid resonances at $N_z^2=S$ corresponding to Fig. 3(b).

We inferred the fully stripped carbon C^{VI} minority fraction from optical $Z_{\rm eff}$ (at 5236 Å)[19,20] measurements and soft x-ray measurements.[21] Fractions of $n_C/n_H \approx 1\%-2\%$ for Ohmic discharges and $n_C/n_H \approx 2\%-4\%$ for high RF power discharges were estimated and their distributions were taken to be parabolic, consistent with the MIST code[22] model. In the following sections we will display two base cases for comparison, with nominally pure H $n_C/n_H \approx 1.4\%$ during Ohmic discharges, climbing to 3% during RF power injection, as well as a different case with added minority $n_D/n_H \approx 25\%$, which from Eq. (2) is equivalent to $n_C/n_H \approx 4.25\%$.

Better models of the RF wave behavior including kinetic effects were also used, and provided more information about power deposition and the discrete mode structure embedded within the approximations described above. According to elfimov and computer code EPSI-2[12,23] (described in Sec. IV), the plasma heating is predicted and observed to be localized to a small region near the tokamak core, and the expected electron Landau damping is quite large.

A scenario where fast wave antenna fields mode convert to this type of ion–ion hybrid Alfvén resonance is promising for tokamak heating and current drive. In principle, the resonant location can be moved from the core to either edge by adjusting species mix, density profiles, or even k_z in real time[24,25] with our phase tunable antenna array.

III. DESCRIPTION OF HEATING EXPERIMENT

Phaedrus-T is a medium-sized tokamak[26] with a major radius $R_0=0.93$ m, minor radius $a=0.25$ m, with a central electron temperature $T_e(0) \approx 400-600$ eV. For this experiment we operated the device with a plasma current of $I_p \approx 70$ kA, edge $q(a) \approx 3.7$, line-average density $\langle n_e \rangle \approx 8\times 10^{18}$ m^{-3}. In the Phaedrus-T tokamak a two strap fast wave antenna array consisting of two toroidally spaced poloidal current straps is used to drive low phase velocity wave fields. For the peak in the vacuum k_z spectrum, the wave phase speed $v_{\phi z}=\omega/k_z$ is substantially less than the core electron thermal speed $v_{\phi z} \approx 0.2-0.3 v_e$, where the electron speed $v_e=(T_e/m_e)^{1/2}$, corresponding to a parallel refraction index $N_\parallel \approx 150$.

The antenna straps were operated at a frequency of 7 MHz with strap phasing of $\phi_{\rm ant}=[0,\pi]$ with a measured peak and minimum of the vacuum k_z spectrum at $k_z \approx 0.2$ and 0.0 cm^{-1}, respectively. We observed electron core heating of 15%–30%, along with a 15%–25% drop in loop voltage. The evanescent wave fields penetrate into the plasma, approximately as $e^{-{\rm Im}(k_z)r}$. Where the density is high enough, the local Alfvén speed can match the launched pump field $v_{\phi z}$ and mode conversion can occur. These mode converted waves also have slow phase speed and are predicted to be a shear Alfvén wave[9,13–15] (SAW) or a mostly electrostatic wave, such as the kinetic Alfvén wave (KAW). The KAW is predicted to have substantial Landau damping onto the large population of subthermal electrons, so that single pass absorbtion of wave power could be quite high. The Ion Bernstein Waves (IBW), which can occur between ion cyclotron harmonics of a multi-ion species plasma are analogous to the KAW in the ion–ion hybrid region.

IV. AW HEATING AND COMPUTER CALCULATION

In Fig. 4 we show the ICRF power $P_{\rm RF}$ gating on with 330 kW average power during the time $t=100-150$ ms. The plasma current is regulated by a feedback system, so that the loop voltage V_L drops promptly some 15%–20%, while the plasma current I_p and the interferometer line density change only slightly. Soft x-ray (SXR) signals show increased sawtooth activity[7] compared with a similar shot with no RF power. In Fig. 5 we display an inset where the time scale is expanded between $t=110-130$ ms and the SXR sawtooth behavior is easier to see.

In a similar series of shots the electron temperature as measured by Thomson scattering increases 15%–30% in the core, and also increases somewhat at $r/a>0.6-0.7$, as shown in Fig. 6(a). The drop in V_L is consistent with the volume-averaged change in T_e of 15%–20% and the associated decrease in Spitzer resistivity, the increase in $Z_{\rm eff}$, along

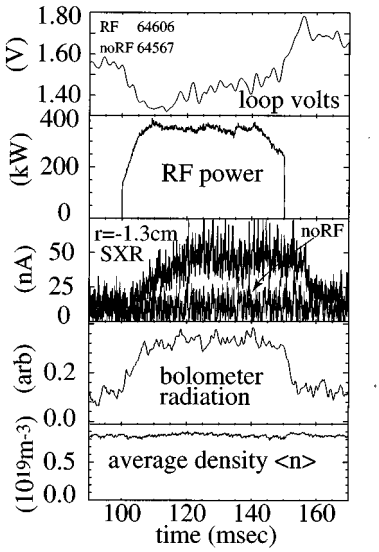

FIG. 4. Typical shot data for nominally pure H^+. From top to bottom we show the time history of loop voltage, RF power P_{RF}, soft x-ray emission SXR for shots with and without RF, total emitted radiation detected by bolometer, interferometer measured line-averaged density.

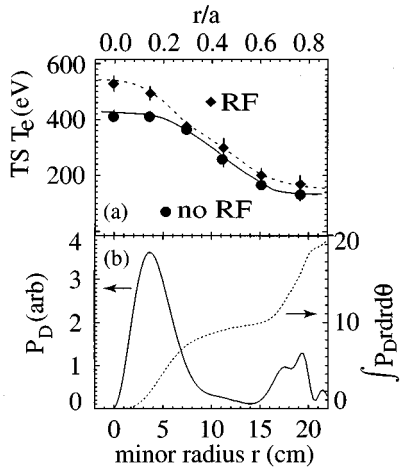

FIG. 6. Electron heating shown by (a) the Thomson electron temperature $T_e(r)$ profile for a series of shots with (diamonds) and without (filled circles) RF power, where $B_0=0.67$ T, $f_{RF}=7$ MHz, $P_{RF}=330$ kW coupled, $\langle n_e\rangle=8\times10^{18}$ m^{-3}. (b) Calculated radial RF power density deposition P_D (solid line) from the one-dimensional cylinder boundary fully kinetic wave code EPSI-2. Integrated flux $\int_0^r\int_0^{2\pi}P_D(r)r\,dr\,d\theta$ in the form of a transmission coefficient is shown by the dashed line. Plasma parameters identical to Fig. 2(a), with $1<q(r)<3.4$, $n_C/n_H=0.032$, $-9<n<0$, $m=-1$, $\phi_{RF}=[0,\pi]$.

with some current drive.[12,19,20,23] The plasma loading is approximately 200–300 mΩ, in addition to vacuum loading of approximately 80 mΩ per strap.

For our Alfvén wave heating and current drive experiments, we desire an estimate of the fraction of P_{RF} coupled to the plasma stored energy. Since we do not have many profile diagnostics in place, we make a crude estimate by assuming that the energy confinement deteriorates as with L-mode scaling.[19,20,27] Then additional energy coupled by adding more P_{RF} only scales as (total power)$^{1/2}=(P_{Ohm}+P_{RF})^{1/2}$. For Ohmic shots with no P_{RF}, $P_{Ohm}\approx110$ kW with an estimated[28] Goldston energy confinement time $\tau_E\approx3.2$ ms. At the time of the Thomson scattering measurements, the RF power input was approximately $P_{RF}\approx330$ kW, with Ohmic power $P_{Ohm}\approx90$ kW, so that τ_E (during RF)≈1.9 ms. Using the data in Fig. 6(a) and assuming $T_i\approx0.6T_e$, we estimate the stored energy for Ohmic shots to be $W_{Ohm}\approx350$ J and for RF shots $W_{RF}\approx430$ J. At the reduced τ_E (during RF), 170 J of the increased stored energy is due to Ohmic heating and the 260 J balance must be due to RF, requiring 260 J/1.9 ms=137 kW. From this, we infer that approximately 40% of the P_{RF} couples to the volume-averaged change in energy density.

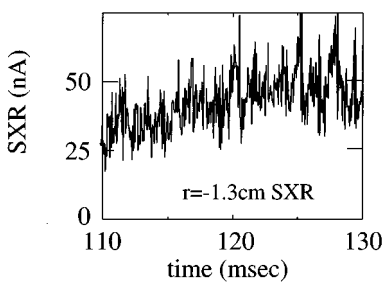

FIG. 5. Inset from Fig. 4 SXR data for the smaller time interval 110–130 ms, showing the sawtoothing behavior near the axis.

To model the wave power deposition we used a computer code EPSI-2[12,23] that calculates the boundary-valued problem for a plasma cylinder with pertubative treatment of the poloidal equilibrium magnetic field due to the plasma current. In this one-dimensional model, kinetic effects are included along with finite Larmor radius effects. We presumed a 3% C^{VI} impurity with a parabolic density profile and the electron temperature radial profiles guided by the Thomson scattering electron temperature (TS T_e) results. A calculated radial power density deposition profile is shown in Fig. 6(b) (solid line) that is very similar to the TS T_e. The heating is predicted to follow from mode converted discrete Alfvén ion–ion hybrid modes and Landau damping on electrons. The radially integrated flux is indicated by the dashed line in Fig. 6(b).

Even though the predicted RF power deposition is hollow near the axis, the experimental data shows that the T_e profile is either slightly peaked or flat inside of $r\approx5$ cm. In general equilibrium, T_e profiles tend to be very similar, or exhibit ''profile consistency,'' even for differing auxiliary heating regimes.[29] For off axis heating, diffusive transport should lead to a temperature profile that is flat inside the heating radius. We speculate that there may be some inward heat pinch, as well as outward diffusive heat flux, similar to the examples shown in the DIII-D tokamak with off axis ECH heating.[30] There is also a predicted RF power deposition near the edge at $r\approx15$–20 cm but little increase in T_e there. One reason may be that radial heat diffusion is typically much higher at the edge than at the core,[29] especially with the addition of auxiliary RF power that is coupling through the edge.

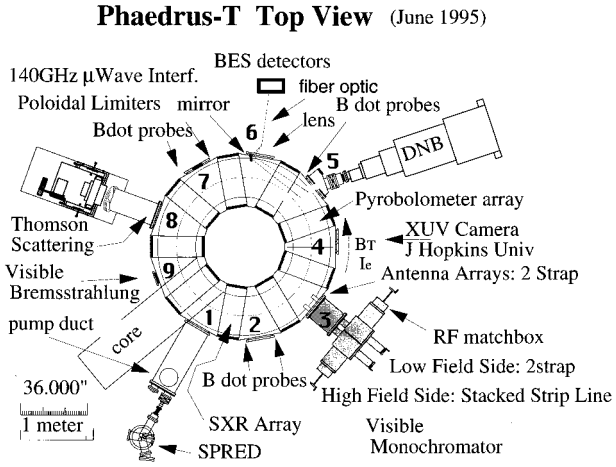

FIG. 7. Schematic of the Phaedrus-T tokamak showing locations of low-field side two strap RF antenna (port box 3), DNB in port (port box 5), and BES diagnostic geometry (port box 6), B-dot probe locations (port box 2), and Thomson scattering (port box 8). Port box numbering is indicated in boldface and the toroidal magnetic field is parallel to the Ohmic electron plasma current indicated near port box 4.

We used beam emission spectroscopy (BES)[31] along with a diagnostic neutral beam (DNB) to view ICRF perturbed ion density changes that were presumed to be caused by the local RF power deposition. The DNB was injected toroidally and the intersection with the BES optics field of view provided a local detection volume of ± 0.5 cm radially, ± 0.25 cm poloidally, and ± 6 cm toroidally for each of the six available BES channels. A schematic of tokamak geometry including antenna, DNB, BES, and toroidal field direction is shown in Fig. 7. The BES signal is sensitive to ion density (mostly) and electron density (somewhat). The RF power was square wave modulated, with varying periods from 2–11 ms during the RF and DNB pulse duration. The pulse modulation periods τ_{RF} were of the order of the energy and particle confinement times, to maximize the observable ion density modulation. To interpret this experiment, only minimal assumptions need to be invoked about the plasma physics inside the tokamak. We assumed that the RF power, if it couples to the plasma, will heat up the plasma electrons and/or ions, and increase the local electron and ion diffusivity, as is usual for L-mode confinement, and deplete the local ion density.

Amplitudes for cross-correlation between RF pump power P_{RF} and BES response V_{BES} were calculated from the time histories of P_{RF} and V_{BES} using a correlation function, defined as

$$C(\Delta t)=\int P_{RF}(t-\Delta t)V_{BES}(t)dt, \tag{7}$$

as a function of the positive causal delay time Δt. Here $C(\Delta t)$ can have positive or negative peaks that correspond to maximum positive correlation or negative anticorrelation for a given Δt. There is some ambiguity inherent in data resulting from correlations such as Eq. (7). For example, it is difficult to tell for repetitive RF power pulses whether negative P_{RF} transitions generated negative correlations (i.e., decrease $P_{RF}\rightarrow$increase in V_{BES}) promptly or positive correlations (i.e., decrease $P_{RF}\rightarrow$decrease in V_{BES}) at some Δt half a square wave period later. To resolve these types of ambiguities, different datasets were taken with different modulation times, including sequential power modulation pulses with time durations at high and low RF power that were not integer multiples of each other.

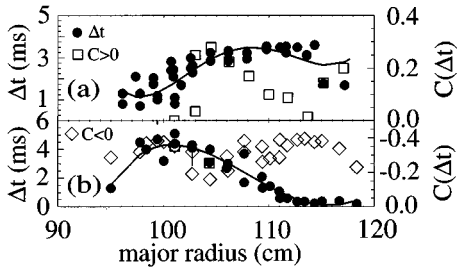

FIG. 8. Radial dependence of correlations calculated from BES data, where the line of sight of each particular channel intersects the DNB path. (a) Positive correlation amplitudes $C(\Delta t)>0$ are shown by the squares, with filled circles indicating the corresponding causal correlation times $\Delta t>0$, showing a positively correlated pulse propagating inward from the antenna side or low field side edge toward the core. (b) Negative correlation amplitudes $C(\Delta t)<0$ are shown by the diamonds with filled circles, indicating the corresponding $\Delta t>0$, showing a negatively correlated pulse propagating outward from the core to the low-field side edge.

Delay times Δt corresponding to peak positive correlation amplitudes for many spatial positions is plotted (filled circles) versus the major radius in Fig. 8(a), along with a curve fitted line. An increase of Δt toward the outside corresponds to outward propagation of correlation pulses. The associated correlation amplitudes $C(\Delta t)>0$ (squares) increase near $R=102-108$ cm. Since the DNB does not penetrate to the core, the decrease of $C(\Delta t)$ in the core and also its peakedness off axis may be exaggerated. Scatter of correlation times Δt in the core is also large. Figure 8(b) shows Δt (filled circles) corresponding to the peak negative correlation as a function of major radius, and implies inward propagation of anticorrelation pulses. Anticorrelation amplitudes $C(\Delta t)<0$ (squares) are plotted as well, and presumably indicate density depletion pulses propagating inward. Anticorrelations peak at the edge at $R=115-118$ and possibly near the core at $R=98-103$ cm. The antenna limiter is on the low-field side and located at $R=119$ cm.

The BES data do not prove the existence of RF heating, but do indicate some RF related phenomena localized to the core region. This combination of edge and core coupling is expected theoretically.[12,23] The notion of an inward propagating pulse is not without precedent. One example we alluded to above is the observation of during electron cyclotron resonance heating on the Doublet III tokamak[32] DIII-D by Luce *et al.* of a nondiffusive electron heat transport mechanism,[30] radially inward against the gradient in T_e. It may be useful for other tokamak CD experiments to take advantage of the radial localization we observe here.

V. FREQUENCY SWEEP EXPERIMENT

A. Experimental description

In order to investigate the wave physics, we performed low RF power experiments[33] on standard Ohmic tokamak

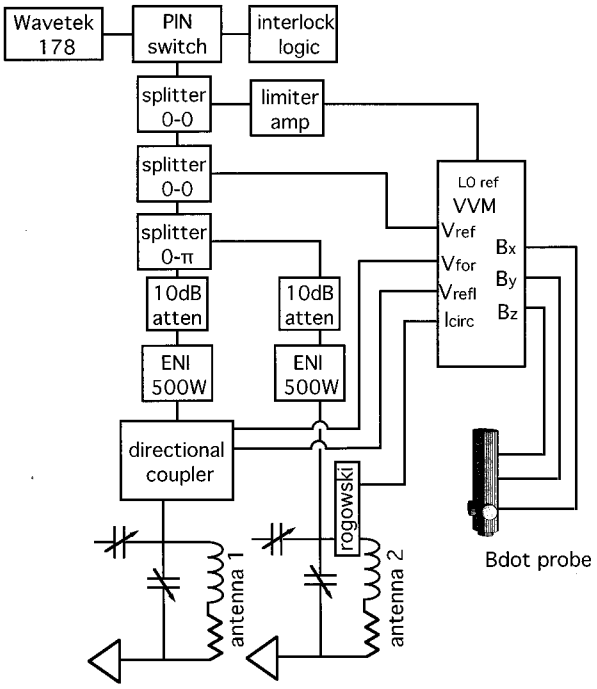

FIG. 9. Schematic of the RF drive chain used to excite two straps of the RF antenna, along with the vector volt meter and local reference oscillator. A B-dot wave probe is also shown schematically.

discharges, with the fast wave antenna array elements phased to $[0,\pi]$, and swept the frequency from far below to above ω_{cH}. Four 30 ms sweeps consisting of a 20 ms sweep plus 10 ms of dead time were carried out per shot. The 200 ms tokamak shot typically had a plasma flat top period of 100 ms, so that at least several of the sweeps had usable data. The frequency tracking linearity of the sweep was verified by directly digitizing the frequency sweep time record. Typical frequency resolution was set by the digitizer sample rate of 40 ksample/s, which for a 2–10 MHz sweep over 20 ms corresponded to a 10 kHz change in sweep frequency during each sample.

As shown in Fig. 9, the frequency source was a Wavetek 178 frequency sweepable signal generator, power split to provide both a local oscillator reference for a broadband (RF $=$2–20 MHz, IF bandwidth$=$40 kHz) vector volt meter and RF driver signal for a low-power (Anzac HH107, 2–35 MHz) 0°–180° hybrid splitter. The split signal drove two broadband power amplifers (ENI A-500, 500 W, gain$=$60 dB, 0.3–35 MHz, 500 W), which excited the two antenna straps through matched lengths of RG17 cable with $[0,\pi]$ phasing.

The antennae were driven through a voltage measurement feedpoint, inserted so as to avoid the series matchbox capacitor, and drive the parallel combination of the strap inductance and parallel matching capacitor directly. The parallel capacitor was adjusted to the minimum value so that the resonance was at the highest possible frequency ($>$25 MHz), and the antenna load was primarily inductive, with $L\approx 700$ nH per strap. The real part of the impedance was due to the small plasma loading, and a typical impedance at 7 MHz was $Z\approx 0.3\ \Omega + j30\ \Omega$.

Amplitudes and phases of the antenna drive signals, antenna circulating currents, and B-dot probes[32] in the plasma were monitored. Group delays $\tau_G = \partial\phi/\partial\omega$ derived from signal phase $\phi(\omega)$ corresponding to cable length and electronic delays were measured as a function of frequency, and were normalized out of the phase measurements. Circulating current was of the order of $4A_{\rm rms}$, and B-dot probe signals were typically normalized to the excitation antenna current $I_{\rm circ}$.

Wave magnetic fields were measured with B-dot[33] probes at a minor radius of $r=22.5$ cm, 2.5 cm on the plasma side of the limiter. Assuming that there were damped waves propagating as

$$B(\omega,k_z;z)\approx Be^{-i[\omega t+m\theta+k_z(\omega)z]}=Be^{-i\phi(\omega)}, \tag{8}$$

we inferred a complex-valued $k_z(\omega)=\mathrm{Re}(k_z)+i\cdot\mathrm{Im}(k_z)$ from the signal phase and amplitudes ensemble averaged over many shots. From the phase shifts of the shear field component B_θ we measured the average values of the wave dispersion properties $k_z(\omega)$. Statistical properties of the collective modes, wave dispersion, and damping properties were accessible by ensemble averaging the realizations over many tokamak shots, and multiple sweeps within shots.

B. Frequency sweep data

Even though the fast wave antenna is nominally a compressional B_z launcher, substantial shear fields are launched[25] and the shear Alfvén wave (SAW) we seek has principally shear polarization. Near the Alfvén resonance zone, the wave group speed slows down and the B_θ wave energy ''piles up'' and swells. Historically the experimental signature of Alfvén waves, even at the core of a largely inaccessible plasma, has been observed to be the edge B_θ wave field,[9,34,35] so our use of edge B-dot probes to measure core wave properties has some tradition behind it.

In a low-power experiment the fast wave antenna array was frequency was swept (e.g., 2–20 MHz) from far below to above ω_{cH}. Magnetic wave fields were measured with B-dot probes[34] inside the low-field side limiter, i.e. in the plasma on the equatorial plane, approximately 90 cm toroidally from the antenna array. We inferred the wave number with a two probe $k_z(\omega)$ measurement, where k_z was assumed to be the phase difference divided by the probe separation along a toroidal arc. We note that the phase speed $v_{\phi z}=\omega/k_z$ as well as the group speed $\mathbf{v}_G=\partial\omega/\partial\mathbf{k}$ can be inferred from frequency swept data. In this case, the direction from the antenna to the B-dot probes corresponded to $k_z<0$, where $k_z>0$ would be parallel to the background B_0 field and antiparallel to the plasma (ion) current.

Representative frequency sweeps in Fig. 10 for strap phasing $\phi_{\rm ant}=[0,\pi]$ show spiky high quality factor $Q>100$ peaks above $\omega > \omega_{cH}(r=0)$ that dominate B_z (not shown) and B_θ (shown). These peaks are the signature of cylinder eigenmodes of the fast magnetosonic (FM) wave. For Fig. 10(a) data, $B_0(0)=0.8$ T, so that $f_{cH}(0)=12.1$ MHz, and for Fig. 10(b), $f_{cH}(0)=10.6$ MHz, where the core and edge $f=f_{cH}$ and harmonic $f=2f_{cH}$ are indicated by arrows. The frequency regions for FM eigenmodes appear to have lower bounds consistent with the core $f_{cH}(0)$. The amplitudes of B_θ and B_r from B-dot probes show broad low $Q<5$ reso-

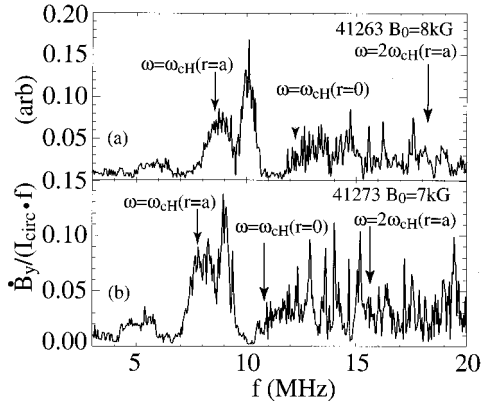

FIG. 10. Frequency swept data showing amplitude of the shear B_θ field for estimated $n_C/n_H=1.4\%$ as a function of frequency for two values of $B_0=0.7$ and 0.8 T. The gyrofrequencies on axis ω_{cH} and at the low-field side edge are shown, and the fast magnetosonic wave cylinder eigenmodes are also evident above $\omega/\omega_{cH}>1$.

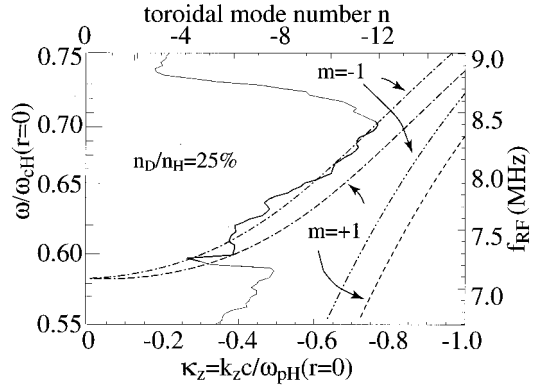

FIG. 12. Axial wave number k_z and toroidal mode number for the low-power sweep experiment with $B_0=0.8$ T, $\langle n_e\rangle=8\times10^{18}$ m^{-3}, estimated $n_D/n_H=25\%$. Wave number k_z is inferred from B-dot B_θ data, and is shown for frequency swept datasets as a dispersion plot of normalized frequency ω/ω_{cH} on the hybrid branch above $\omega/\omega_{cH}>\omega_{ii}$ versus normalized wave number $\kappa_z=k_zc/\omega_{pH}$.

nances below $\omega_{cH}(r=a)$, where the ion gyrofrequency enters the low-field side edge. Representative frequency sweeps with $\phi_{ant}=[0,0]$ (not shown) indicate a very small τ_G corresponding to a B_θ group speed too large to measure with a lower limit of $v_G>10^9$ cm/s. For these $\phi_{ant}=[0,0]$ data we measured $k_z\approx0.055$ cm^{-1}, approximately independent of frequency in the range 5 MHz$<f_{RF}<$9 MHz.

For a nominally pure H plasma with $\phi_{ant}=[0,\pi]$, the results of an ensemble-averaged $k_z(\omega)$ measurements are shown in Fig. 11(a), where toroidal mode number $n=k_zR_0<0$ is indicated on the top axis and normalized wave number $\kappa_z=k_zc/\omega_{pH}(r=0)$ on the bottom. Frequency is normalized to $\omega_{cH}(r=0)$. The theoretically expected dispersion from Eq. (3) for the pure H Alfvén continuum with $m=-1$ is indicated with a dotted line. The split hybrid Alfvén continuua from Eq. (6), including our actual impurity fraction of 1.4% carbon, is shown by the dashed lines for the resonance $N_\parallel^2=S$. The two branches above (hybrid) and below (Alfvénic) ω_{ii} are apparent in Fig. 11(a), along with the gap in between. The hybrid branch asymptotes to $\omega=\omega_{ii}$ at small $|k_z|$ and the Alfvén branch asymptotes to $\omega=0.5\omega_{cH}$ at large $|k_z|$.

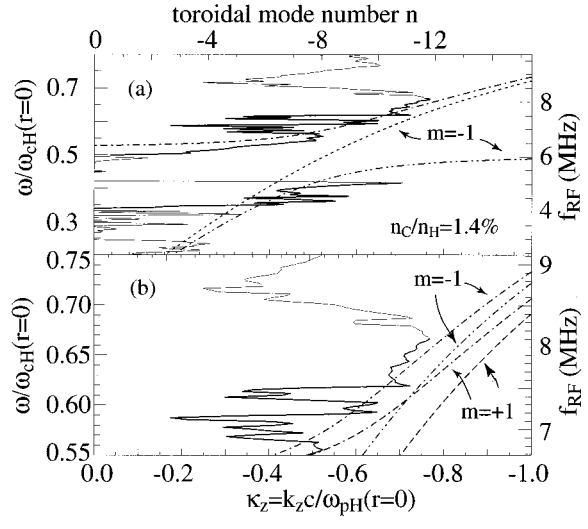

FIG. 11. Axial wave number k_z and toroidal mode number for the low-power sweep experiment with $B_0=0.8$ T, $\langle n_e\rangle=8\times10^{18}$ m^{-3}, estimated $n_C/n_H=1.4\%$. (a) Here k_z is inferred from B-dot B_θ data, and is shown for frequency swept datasets as a dispersion plot of normalized frequency ω/ω_{cH} versus normalized wave number $\kappa_z=k_zc/\omega_{pH}$. The Alfvénic branch below ω_{cD}, i.e., $\omega/\omega_{cH}<0.5$ and the hybrid branch above the ion–ion hybrid frequency ω_{ii}, i.e. $\omega/\omega_{cH}\approx0.55$ are evident. (b) The dispersion plot is shown with an expanded frequency scale to show the hybrid branch in more detail.

In Fig. 11(b) we show the phase data from these probes along with calculations, but for an expanded scale in the region of interest. The measured dispersion fits approximately in the region for the cylinder fluid model of Eq. (6), where the range in $k_z(k_\parallel)$ corresponding to the $-1<m<+1$ range in poloidal mode number is shown in Fig. 11(b).

Figure 12 shows the same type of data set as Fig. 11(b) for a dispersion curve displayed as $\omega/\omega_{cH}(r=0)$ vs $k_zc/\omega_{pi}(r=0)$, but for a substantial fraction of D impurity, $n_D/n_H=25\%$. The vertical scale has been expanded to show the region of interest and dispersion of the hybrid branch. The dispersion curve has moved upward in frequency, with the gap now below $\omega\approx0.6\omega_{cH}(r=0)$, as expected. In a forthcoming paper,[36] we will show from measured toroidal damping that there is a discrete eigenmode structure embedded in the dispersion data of Figs. 11 and 12. This turns out to be consistent with our identification of the waves as Alfvénic ion–ion hybrid modes.

VI. DISCUSSION

For plasma heating or current drive we would like to maximize the fraction of RF power coupled or at least establish some estimate of the power balance. If, as suggested in Sec. IV, the energy confinement deteriorates as L-mode scaling[19,27,28] approximately 40% of the P_{RF} power is coupled to the increase in T_e. The rest may be appearing as current drive or is otherwise unaccounted for. Our conclusion that the waves responsible are an Alfvénic ion–ion hybrid

mode is supported both by the dispersion relation data and predicted core RF power perturbations, as measured by BES that give rise to core heating, as measured by TS T_e profiles.

The dispersion relation data of in Figs. 11 and 12 show the two theoretically expected Alfvénic ($\omega < \omega_{cD}$) and ion–ion hybrid ($\omega > \omega_{ii}$) branches[12] [cf. Eq. (6)], with a gap in between ($\omega_{cD} < \omega < \omega_{ii}$). The upper edge of the gap frequency increases with minority concentration, as it should according to Eq. (2). Figure 11 also shows the existence of backward propagating waves in the ''forbidden'' frequency gap, $\omega_{cD} < \omega < \omega_{ii}$, that turn out to be highly damped or evanescent in the toroidal direction. These backward waves are not allowed for in the cylinder or slab model but may exist in the edge or from toroidal effects. Figure 12 shows a similar trend, but the k_z and wave amplitudes only get small and k_z does not appear to switch sign. We defer the discussion of why the edge measurement of the shear wave phase is a robust indicator of Alfvénic wave structure, and how the damping is connected with a discrete eigenmode structure embedded in the dispersion data of Figs. 11 and 12 to another paper.[36] The discrete eigenmode spectrum[36] also turns out to be consistent with our identification of the waves as Alfvénic ion–ion hybrid modes. A recent thesis study by Vukovic[37] using a two-dimensional toroidal cold plasma code and radially localized microwave scattering information from reflectometer data also corroborates this conclusion.

The kinetic cylinder model EPSI-2 can account for the radially localized power deposition profiles that are consistent with the TS T_e data, showing a core temperature increase with RF power. With BES we measure outwardly propagating pulses that are correlated with the RF power and probably the core heating we observe due to mode converted Alfvénic waves. BES also indicates inwardly propagating pulses that are anticorrelated with the RF power that may be associated with the directly driven edge waves and scrape-off layer perturbations excited by the RF antenna.

In the search for electron current drive schemes, waves with low parallel phase velocity are ideal candidates because they interact with the large bulk electron distribution. The few choices consist of ion Bernstein waves (IBW), Alfvén waves (AW), kinetic Alfvén waves (KAW), and the Alfvénic ion–ion hybrid waves discussed in this paper. In the usual Stix notation, the notion of a $k_r \rightarrow \infty$ perpendicular resonance at some $N_\parallel^2 = S$ location holds equally well for the well-known Alfvén resonance, and the ion–ion hybrid resonance. In these cases the IBW can appear near harmonics of the heavier species, so these waves are all related at the $N_\parallel^2 = S$ resonance. In fact, the more familiar Buchsbaum–Bers[16] ion–ion hybrid resonance is the parallel cutoff limit ($k_\parallel \rightarrow 0$, $S = 0$) of the general finite $k_\parallel \neq 0$ case, i.e. the Alfvénic ion–ion hybrid mode. For larger tokamaks such as TFTR,[11] where ion–ion hybrid mode conversion scenarios have been exploited, the IBW probably plays a role in resolving the resonance. These are higher-order kinetic processes that are beyond the purview of the kinetic code EPSI-2 used in this paper. Even if a higher-order calculation was necessary to resolve the magnitude of the damping, these details do not affect the calculated radial locations of the damping.

The connection between the Alfvén and hybrid modes is known but not generally appreciated. This is much more apparent when viewed from the standpoint of the dispersion diagrams, such as shown in Figs. 11 and 12 than it is when one looks at a radially localized wave behavior and wave number in the sheared tokamak geometry. The dispersion diagrams suffer the drawback that they follow from cylindrical boundary-valued models with the sheared $B = B_0 + B_\theta(r)$ field treated as a perturbation. On the other hand, since the cylinder model has averaged in some sense over radius, global behavior is displayed.

Hybrid effects on the Alfvén spectrum have recently received some attention,[11] and mode conversion to an ion–ion hybrid Alfvén resonance may be very useful for spatially localized tokamak heating and current drive. Borg and Cross[38] may have observed a similar hybrid wave with a cold, light ion minority plasma, but did not measure any dispersion, discrete mode characteristics, or heating.

VII. CONCLUSION

We have carried out two related experiments on the Phaedrus-T tokamak, and have measured core localized RF power deposition with electron heating, and also found the signature of a mode converted Alfvén ion–ion-hybrid wave. We show that small fractions of minority ions can have a large effect on the Alfvén spectrum, as measured at the edge. We have used a low-power frequency sweeping technique and experimentally identified the ion–ion hybrid Alfvén wave.

For this hybrid regime near $\omega \approx \omega_{ii}$, a small frequency range can excite a large range of k_z, and offer a promising route to spatially adjustable tokamak heating and current drive, by adjusting species mix, density profiles, or k_z.[24] Radial localization of the RF power deposition demonstrated here may turn out to be useful for off axis current drive tokamak experiments. Edge current drive can drive reversed shear in the safety factor (q), which also appears to lead to desirable reduced radial transport properties.[39]

Computer models of the hybrid Alfvén spectrum predict resonance locations in Phaedrus-T that are consistent with the experimental Thomson scattering electron heating profiles and BES correlation pulse data we measure, as well as the measured discrete eigenmode spectrum. At an aspect ratio of 3.7 this tokamak has significant toroidicity, yet a cylindrical model appears to sufficiently explain the data shown in this paper. The mode conversion waves occur in the core plasma that has a large local aspect ratio, and may be why the perturbative treatment of toroidicity is adequate.

Alfvén ion–ion hybrid effects are the necessary result of impurity ion species, and affect the interactions of these Alfvénic waves with plasma electrons. A number of laboratory measurements, including Alfvén resonant heating[7,8] antenna loading,[9] and wave fields in tokamaks[10] that have been carried out with nominally ''pure'' hydrogen plasmas, may actually have been studies of the Alfvén ion–ion hybrid waves. These comments are not restricted to H-minority plasmas, because even plasmas with a nominal D fill gas and partially stripped impurities will still exhibit these Alfvén-hybrid properties, although probably only on the edge.

In the Phaedrus-T tokamak Alfvén waves are indirectly driven by a conventional fast wave antenna array, and generate electron heating in the plasma core. The general picture of the dispersion relation we show in Figs. 11 and 12 holds for nonhydrogen plasmas as well. For example, in a He^3–T plasma the Alfvénic mode is below the lower gyrofrequency $\omega_{c\mathrm{T}}$, the Alfvén ion–ion hybrid mode is below the upper gyrofrequency $\omega_{c\mathrm{He}}$.[3] The ion–ion hybrid frequency ω_{ii} will be above $\omega_{c\mathrm{T}}$ and below $\omega_{c\mathrm{He}}$.[3] This is an alternative view of the type of mode conversion current drives scenario[11] that has been shown to work in TFTR. We view the modes at fixed $k_\perp$ and vary k_z, instead the conventional view of radially varying dispersion $k_\perp$ as a function of fixed k_z.

We have pointed out that finite k_z changes the Buchsbaum–Bers perpendicular hybrid resonance ($k_z=0$) to one that couples the Alfvénic, ion–ion hybrid and a third electrostatic (either KAW or IBW) waves intimately. Scenarios where fast wave antenna fields mode convert to an ion–ion hybrid Alfvén resonance promise a route to tokamak heating and current drive. For the Alfvén spectrum at least, theories predicated on the presumption of one pure ion species may be unrealistic for tokamaks. For hydrogen plasmas where impurity fractions leading to a $Z_{\mathrm{eff}}\approx 1.3$–$2$ are the rule rather than the exception, small impurity fractions can have a large effect on the wave properties.

ACKNOWLEDGMENT

This work was supported by the United States Department of Energy, Grant No. DE-FG02-88ER53264.

[1] J. Tataronis and W. Grossman, Z. Phys. **261**, 203 (1973).
[2] L. Chen and A. Hasegawa, Phys. Fluids **17**, 1399 (1974).
[3] D. W. Ross, G. L. Chen, and S. W. Mahajan, Phys Fluids **25**, 652 (1982).
[4] J. M. Davila, Astron. Astrophys. **317**, 514 (1987).
[5] A. Hasegawa and L. Chen, Phys. Fluids **19**, 1924 (1976).
[6] R. L. Lysak and C. T. Dum, J. Geophys. Res. **88**, 365 (1983).
[7] R. Majeski, P. H. Probert, P. Moroz, T. Intrator, R. Breun, D. Brouchous, H. Y. Che, J. R. DeKock, D. Diebold, M. Doczy, R. Fonck, N. Hershkowitz, R. D. Johnson, M. Kishinevsky, G. McKee, J. Meyer, P. Nonn, S. P. Oliva, J. Pew, J. Sorenson, T. Tanaka, M. Vukovic, and G. Winz, Phys. Fluids B **5**, 2506 (1993).
[8] B. Joye, A. Lietti, J. B. Lister, J. M. Moret, and W. Simm, Phys. Rev. Lett. **56**, 2481 (1986).
[9] G. A. Collins, F. Hoffman, B. Joye, R. Keller, A. Lietti, J. B. Lister, and A. Pochelon, Phys. Fluids **29**, 2260 (1986).
[10] A. B. Murphy, Nucl. Fusion **31**, 465 (1991).
[11] R. Majeski, C. K. Phillips, and R. Wilson, Phys. Rev. Lett. **73**, 2204 (1994).
[12] A. Elfimov, J. Tataronis, and N. Hershkowitz, Phys. Plasmas **1**, 2637 (1994).
[13] R. C. Cross, *An Introduction to Alfvén Waves* (Hilger, Institute of Physics Publishing, Bristol, UK, 1988).
[14] See National Technical Information Service Document No. DE-82001702 (A. Hasegawa and C. Uberoi, *The Alfvén Wave*). Copies may be ordered from the National Technical Information Service, 5285 Fort Royal Road, Springfield, VA 22161.
[15] J. Vaclavik and K. Appert, Nucl. Fusion **31**, 1945 (1991).
[16] S. J. Buchsbaum, Phys. Fluids **3**, 418 (1960).
[17] N. F. Cramer and C. M. Yung, Plasma Phys. Controlled Fusion **28**, 1043 (1986).
[18] T. H. Stix, *Waves in Plasmas*, 2nd ed. (American Institute of Physics, New York, 1992).
[19] T. Intrator, P. Probert, S. Wukitch, M. Vukovic, D. Brouchous, D. Diebold, R. Breun, M. Doczy, D. Edgell, A. Elfimov, N. Hershkowitz, M. Kishinevsky, C. Litwin, P. Moroz, P. Nonn, and G. Winz, Phys. Plasmas **2**, 2263 (1995).
[20] S. Wukitch, M. Vukovic, R. Breun, D. Brouchous, D. Diebold, M. Doczy, A. Elfimov, D. Edgell, N. Hershkowitz, T. Intrator, M. Kishinevsky, C. Litwin, P. Moroz, and P. Probert, Phys. Rev. Lett. **74**, 2240 (1995).
[21] S. P. Regan, M. Finkenthal, M. J. May, and H. Moos, Rev. Sci. Instrum. **66**, 770 (1995).
[22] R. A. Hulse, Nucl. Technol. Fusion **3**, 259 (1983).
[23] A. G. Litvak, in *High Frequency Plasma Heating, Alfvén Wave Heating and Current Drive* (American Institute of Physics, New York, 1992), p. 239, Chap. IV.
[24] R. Majeski P. Probert, T. Tanaka, D. Diebold, R. Breun, M. Doczy, R. Fonck, N. Hershkowitz, T. Intrator, G. McKee, P. Nonn, J. Pew, and J. Sorensen, Fusion Eng. Design **24**, (1994).
[25] N. Hershkowitz, R. Majeski, T. Tanaka, and T. Intrator, in *Radio Frequency Power in Plasmas*, Proceedings of the 8th Topical Conference, Irvine, 1989, AIP Conf. Proc. 190 (American Institute of Physics, New York, 1989), p. 270.
[26] R. A. Breun, D. Brouchous, D. Diebold, R. Fonck, N. Hershkowitz, T. Intrator, Y. J. Kim, M. Kishinevsky, W. Li, R. Majeski, J. Pew, P. Probert, E. Y. Wang, Y. Wen, H. Che, M. Doczy, G. McKee, J. Sorenson, T. Tanaka, M. Vukovic, P. Bellan, and M. R. Brown, Fusion Technol. **19**, 1327 (1991).
[27] T. Intrator, P. Probert, M. Vukovic, M. Harper, S. Wukitch, R. Breun, D. Brouchous, D. Diebold, M. Doczy, D. Edgell, N. Hershkowitz, M. Kishinevsky, C. Litwin, P. Nonn, and G. Winz, ''Alfvén Wave Current Drive Experiments in Phaedrus-T,'' to appear in *Radio Frequency Power in Plasmas*, Proceedings of the 11th Topical Conference, Palm Springs, CA, 17–19 May 1995 (American Institute of Physics, New York, in press).
[28] Energy confinement estimate $\tau_E\approx 1.0\times 10^{-21}\langle n\rangle a^{1.04}R^{2.04}q_a^{0.5}$; from R. J. Goldston, Plasma Phys. Controlled Fusion **26**, 87 (1984).
[29] J. D. Callen, J. P. Christiansen, J. G. Cordey, P. R. Thomas, and K. Thomsen, Nucl. Fusion **27**, 1857 (1987).
[30] T. C. Luce, C. C. Petty, and J. C. M. DeHaas, Phys. Rev. Lett. **68**, 52 (1992).
[31] H. Evenson, D. Brouchous, D. Diebold, M. Doczy, R. J. Fonck, and D. Nolan, Rev. Sci. Instrum. **63**, 4928 (1992).
[32] R. D. Stambaugh, R. W. Moore, L. C. Bernard, A. G. Kellma, and E. J. Sraight, in *Plasma Physics and Controlled Nuclear Fusion Research*, Proceedings of the 10th International Conference, London, 1984 (International Atomic Energy Agency, Vienna, 1985), Vol. I, p. 217.
[33] P. Descamps, G. Van Wassenhove, R. Koch, A. M. Messiaen, P. E. Vandenplas, J. B. Lister, and Ph. Marmillod, Phys. Lett. A **143**, 311 (1990).
[34] T. Intrator, R. Majeski, P. Probert, and M. Vukovic, in *Radio Frequency Power in Plasmas*, Proceedings of the 9th Topical Conference, Charleston, 1991, AIP Conf. Proc. 244 (American Institute of Physics, New York, 1991), p. 319.
[35] R. D. Bengtson, J. F. Benesch, G. L. Chen, T. E. Evans, Y. M. Li, S. H. Lin, S. M. Mahajan, R. B. Michie, M. E. Oakes, D. W. Ross, P. Valanju, and C. M. Surko, *Proceedings of the 3rd Joint International Symposium on Heating in Toroidal Plasmas*, 22–26 March 1982, Grenoble (Commisson of the European Communities, Brussels, 1982), Vol. 1, p. 151.
[36] T. Intrator, M. Vukovic, A. Elfimov, P. H. Probert, and G. Winz, Phys. Plasmas **3**, 10541 (1996).
[37] M. Vukovic, ''Toroidal effects on the Alfvén resonance in the Phaedrus-T tokamak,'' Ph.D. thesis, University Wisconsin, Madison, WI, 1995.
[38] G. G. Borg and R. C. Cross, Plasma Phys. Controlled Fusion **28**, 681 (1987).
[39] M. Zarnstorff and the TFTR Group, Bull. Am. Phys. Soc. **40**, 1747 (1995).